Journal of Power Sources xxx (2016) 1–8

Contents lists available at ScienceDirect

Journal of Power Sources

journal homepage: www.elsevier.com/locate/jpowsour

Organic electrolyte-based rechargeable zinc-ion batteries using potassium nickel hexacyanoferrate as a cathode material

Munseok S. Chae, Jongwook W. Heo, Hunho H. Kwak, Hochun Lee, Seung-Tae Hong*

Department of Energy Systems Engineering, DGIST, Daegu 42988, South Korea

HIGHLIGHTS

- The zinc-ion battery system was demonstrated with an organic electrolyte.
- The organic electrolyte provides higher zinc cycling efficiency than aqueous one.
- The structure of zinc-inserted phase was confirmed with Rietveld refinement.
- The zinc ion positions were determined using Fourier electron-density analysis.

GRAPHICAL ABSTRACT

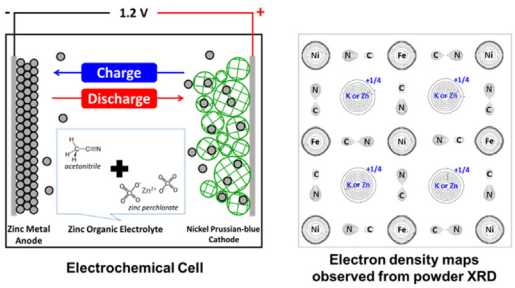

ARTICLE INFO

Article history:
Received 28 July 2016
Received in revised form
26 September 2016
Accepted 23 October 2016
Available online xxx

Keywords:
Prussian blue
Nickel hexacyanoferrate
Zinc-ion battery
Multivalent-ion battery
Crystal structure
Non-aqueous zinc battery

ABSTRACT

This study demonstrates an organic electrolyte-based rechargeable zinc-ion battery (ZIB) using Prussian blue (PB) analogue potassium nickel hexacyanoferrate $K_{0.86}Ni[Fe(CN)_6]_{0.954}(H_2O)_{0.766}$ (KNF-086) as the cathode material. KNF-086 is prepared *via* electrochemical extraction of potassium ions from $K_{1.51}Ni[Fe(CN)_6]_{0.954}(H_2O)_{0.766}$ (KNF-151). The cell is composed of a KNF-086 cathode, a zinc metal anode, and a 0.5 M $Zn(ClO_4)_2$ acetonitrile electrolyte. This cell shows a reversible discharge capacity of 55.6 mAh g^{-1} at 0.2 C rate with the discharge voltage at 1.19 V (vs. Zn^{2+}/Zn). As evidenced by Fourier electron density analysis with powder XRD data, the zinc-inserted phase is confirmed as $Zn_{0.32}K_{0.86}Ni[Fe(CN)_6]_{0.954}(H_2O)_{0.766}$ (ZKNF-086), and the position of the zinc ion in ZKNF-086 is revealed as the center of the large interstitial cavities of the cubic PB. Compared to KNF-086, ZKNF-086 exhibits a decreased unit cell parameter (0.9%) and volume (2.8%) while the interatomic distance of *d*(Fe-C) increased (from 1.84 to 1.98 Å), and the oxidation state of iron decreases from 3 to 2.23. The organic electrolyte system provides higher zinc cycling efficiency (>99.9%) than the aqueous system (ca. 80%). This result demonstrates an organic electrolyte-based ZIB, and offers a crucial basis for understanding the electrochemical intercalation chemistry of zinc ions in organic electrolytes.

1. Introduction

With the emergence of new technologies such as electric vehicles, wearable electronic devices, and renewable energy storage systems (ESS), there is an ever-increasing demand for high performance-batteries [1–3]. Lithium-ion batteries (LIBs) are the most prevalent technology and are superior in respect of energy and power densities. However, with issues such as the safety of lithium-based batteries and the uneven distribution of the lithium reserves over the world, research has shifted focus towards post-LIB technologies [4,5].

* Corresponding author.
E-mail address: st.hong@dgist.ac.kr (S.-T. Hong).

http://dx.doi.org/10.1016/j.jpowsour.2016.10.083
0378-7753/

Rechargeable multivalent ion batteries utilizing magnesium, zinc, calcium, or aluminum ions have received much attention as post-LIB candidates, mainly because of advantages such as the abundance of the constituent elements, their safety, and their potential for higher energy density. In particular, zinc-ion batteries are considered as promising candidates for large-scale ESS applications [6]. Zinc provides various merits in safety, abundance, low cost, environmental friendliness, and large capacity (i.e., zinc metal has a capacity of 820 mAh g^{-1}). Recently zinc was also reported as a component of Zn-Sb intermetallic nanomaterial for an anode material of sodium-ion batteries [7]. However, only a few host compounds enabling electrochemical zinc-ion intercalation have been reported so far: MnO_2 with the hollandite [6], birnessite [8] or todorokite [9] structures, Chevrel phase Mo_6S_8 [10–12], and Prussian blue analogues [13–16].

The derivatives of the cubic Prussian blue (PB) phase have large open-framework structures, as shown in Fig. 1a. With high durability and high redox potentials, these materials have already proven to be good host materials for various cations, including lithium [17], sodium [18–25], potassium [26,27], and divalent ions, e.g., magnesium, calcium, strontium, barium, and zinc in acidic aqueous electrolytes [14,15,28], or nonaqueous electrolyte [16]. An ideal PB derivative without any defects can be simply described as $A_2MM'(CN)_6$ (A = metal ions, zeolitic water; M = Fe, Ni, Mn, V, Mo, Cu, Co; M' = Fe, Co, Cr, Ru). The structure is analogous to that of the double perovskite $A_2BB'O_6$, where B, B′, and O correspond to M, M′, and (C≡N), respectively. M and M′ are ordered to form a face-centered rock-salt arrangement, and the two atoms are connected *via* C≡N, forming an M′–C≡N–M sequence where M and M′ have an octahedral coordination with N and C, respectively. A-site cations, which are usually—but not limited to—alkali metal ions or zeolitic water, occupy the large cavities formed by twelve CN groups. Such cavities form three-dimensional diffusion channels, so that the A-ions or water can be transported easily. The PB-derivatives usually have defects of $Fe(CN)_6$, with the vacant N sites occupied by water molecules. Thus, PB materials are represented by the general formula $A_xM[M'(CN)_6]_{1-y}(H_2O)_z$, where x is the range of the occupancy of A-ions. Typically, x is in the range $0 \leq x \leq 2$, but the existence of zeolitic water can narrow this range. The portion of defects in the $M(CN)_6$ sites is denoted by y in the general formula, with y having the range $0 \leq y \ll 1$. Water molecules are found in the large interstitial sites as well as the defect N sites, and the amount of water, z, is in the range $0 \leq z \leq 2\text{-}x+6y$. That is, z should be equal to or less than the total number of large interstitial sites (2) and defect N sites ($6y$) subtracted by the number of occupied A metals (x).

Thus far, most of the reported electrochemical intercalation experiments have been performed in aqueous electrolytes (i.e., aqueous $ZnSO_4$ or $Zn(NO_3)_2$ solutions). Accordingly, the narrow electrochemical stability window of aqueous electrolytes (ca. 1.2 V) has limited the operating voltage of the host materials. Moreover, in acidic aqueous solutions, protons or hydronium ions (H_3O^+) take part in the intercalation reaction as well as zinc ions [28]. Acidic electrolytes can cause corrosion of metal packaging and current collectors, resulting in poor long-term reliability. On the other hand, alkaline aqueous electrolytes tend to form an insulating zinc oxide (ZnO) layer on the zinc surface, resulting in a low Coulombic efficiency (CE) during the zinc deposition/stripping cycle [6,15]. To exclude these intrinsic issues associated with aqueous electrolytes, we herein studied a zinc-ion battery (ZIB) using an organic electrolyte with the cell consisting of the PB-analogue $K_xNi[Fe(CN)_6]_{1-y}(H_2O)_z$ and zinc metal as the positive and negative electrode materials, respectively, with 0.5 M $Zn(ClO_4)_2$ in acetonitrile (AN) as the organic electrolyte. We report the synthesis of the PB derivative phases as positive host materials, the electrochemical insertion and extraction properties of zinc ions into the host materials, reversible dissolution and deposition of the zinc metal in the organic electrolyte, and finally, structural analyses of the new zinc-inserted phases.

2. Experimental

2.1. Synthesis and electrochemical characterization

Nanoparticles of the PB analogue $K_xNi[Fe(CN)_6]_{1-y}(H_2O)_z$ were synthesized by a simple precipitation method [29]. An aqueous solution of $Ni(NO_3)_2 \cdot 6H_2O$ (94.5–105.5%, Sigma-Aldrich) (10 ml, 1.3 M) was slowly added into an aqueous solution of $K_4[Fe(CN)_6] \cdot 3H_2O$ (98.5–102.0%, Sigma-Aldrich) (20 ml, 0.5 M) with vigorous stirring, immediately producing insoluble colloidal products. The colors of the initial solution and the products were yellow and light green, respectively. After a stirring for 30 min at room temperature, the solution underwent centrifugation at 10,000 rpm for 10 min in order to separate the unreacted reagents from the product, and was subsequently washed with D.I. water three times. However, a small amount of unreacted $Ni(NO_3)_2$ was still observable by powder XRD. Thus, the powder was re-dispersed in 10 ml of 0.5 M $K_4Fe(CN)_6 \cdot 3H_2O$ and 20 ml of D.I. water, and stirred for

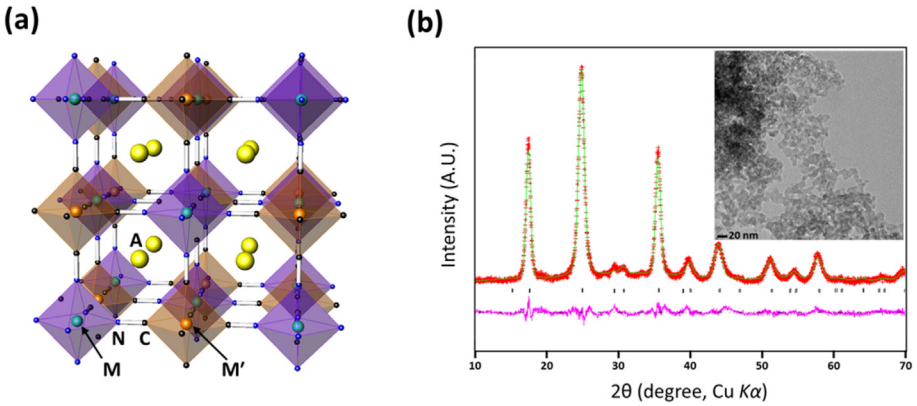

Fig. 1. (a) The unit cell structure of an ideal Prussian-blue phase, $A_2MM'(CN)_6$. (b) Powder XRD Rietveld refinement profile for $K_{1.51}Ni[Fe(CN)_6]_{0.954}(H_2O)_{0.766}$ (KNF-151) recorded at 25 °C, and a TEM image of the particles. Red points: experimental data. Green line: calculated data. Pink line: difference. Black bars: Bragg positions. (For interpretation of the references to colour in this figure legend, the reader is referred to the web version of this article.)

Please cite this article in press as: M.S. Chae, et al., Journal of Power Sources (2016), http://dx.doi.org/10.1016/j.jpowsour.2016.10.083